

Generalized Optimization-based Synthesis of Membrane Systems for Multicomponent Gas Mixture Separation

Garry S.P. Taifan^{a,b}, Christos T. Maravelias^{a,b,c,*}

^a*Department of Chemical and Biological Engineering, Princeton University, 50-70 Olden St, Princeton, 08540, NJ, USA*

^b*DOE Great Lakes Bioenergy Research Center, USA*

^c*Andlinger Center for Energy and Environment, Princeton University, 86 Olden St, Princeton, 08540, NJ, USA*

Abstract

Synthesizing a membrane system to separate multicomponent gas mixture is challenging due to the combinatorial number of feasible configurations and the difficulties in describing the multicomponent permeators. We present a mixed-integer nonlinear programming (MINLP) model for synthesizing membrane systems for multicomponent gas mixture separation. The approach employs a richly connected superstructure to represent numerous potential system configurations, and different physics-based surrogate permeator models, such as countercurrent flow or crossflow, to be used in each stage. Moreover, to describe realistic systems, pressure drop equations can be included. We also present solution methods to accelerate the solution process. Through a case study of natural gas sweetening, we demonstrate that the proposed approach is able to obtain good solutions using an off-the-shelf global optimization solver. Finally, we expand the conventional membrane system

*Corresponding author

Email address: maravelias@princeton.edu (Christos T. Maravelias)

Preprint submitted to Chemical Engineering Science

December 1, 2021

synthesis problem by introducing feed variability in our model through a case study of an integrated reactor-separation system.

Keywords: Global optimization, membrane gas separation, process synthesis

1 Introduction

2 Membranes for gas separation have been considered a promising technol-
3 ogy due to their compactness, energy efficiency, scalability, and flexibility
4 (Koros and Lively, 2012; Humphrey and Keller, 1997). This technology ex-
5 ploits the difference in permeability of substances in a semipermeable barrier
6 to achieve separation. Apart from natural gas processing, air separation, car-
7 bon capture, and hydrogen recovery, membrane-based separations are also
8 implemented in olefin/paraffin separation, H_2/CO_2 separation, helium recov-
9 ery, and biogas treatment (Iulianelli and Drioli, 2020). In the past decades,
10 the adoption of this technology has grown significantly, and, accordingly, sig-
11 nificant research efforts are devoted to membrane material design (Du et al.,
12 2011; McKeown and Budd, 2010; Park et al., 2007; Pinnau et al., 1996). Two
13 important characteristics of membrane materials in relation to separations
14 are permeability and selectivity. High permeability is often associated with
15 high recovery, while increased selectivity is associated with high purity. How-
16 ever, it was found that polymeric membranes, the mostly used materials for
17 industrial gas separation, often exhibit a trade-off between permeability and
18 selectivity, which was summarized in a Robeson plot (Robeson, 2008). Due
19 to this trade-off, employing a single permeation stage for a separation task is
20 often not feasible, and even if it is feasible, it is usually economically unfavor-

21 able due to a high compression cost (Castro-Dominguez et al., 2015; Merkel
22 et al., 2010). To overcome this inherent limitation, several permeators could
23 be interconnected forming a network. As a consequence, the economics of the
24 separation depends critically on the decisions made in the process synthesis,
25 such as the configuration and operating conditions (Qi and Henson, 2000).

26 There are two main approaches to synthesize membrane systems: simulation-
27 based and optimization-based. In general, process synthesis includes two
28 types of decisions: structural (e.g., number of stages) and operational (e.g.,
29 pressure ratio and membrane area in each stage). In simulation-based ap-
30 proaches, structural decisions are fixed and operating decisions are deter-
31 mined through iterative procedures (Agrawal and Xu, 1996; Krovvidi et al.,
32 1992; Murad Chowdhury et al., 2005; Pan, 1983). As more permeation stages
33 are considered, the enumeration of process configurations becomes time-
34 consuming. As a result, only few configurations based on engineering judge-
35 ment and heuristics can be evaluated (Spillman, 1995; Stern et al., 1984).
36 On the other hand, in optimization-based approaches, both structural and
37 operational decisions are determined simultaneously. This is usually done by
38 postulating a superstructure comprising many process configurations (Gross-
39 mann, 1996). A mixed integer nonlinear programming (MINLP) problem is
40 then formulated based on the superstructure, where integer and continuous
41 variables are used to represent structural and operational decisions, respec-
42 tively.

43 Arias et al. (2016) presented a nonlinear programming (NLP) model for
44 multistage membrane systems for carbon capture from flue gas represented
45 as a binary mixture. In their approach, a superstructure with restricted in-

46 terconnections was used where each membrane stage was modeled using a
47 discretization method. The resulting optimization model was solved using a
48 local solver. Ohs et al. (2016) proposed a superstructure with two perme-
49 ation stages for N_2/CH_4 mixture separation, and the resulting optimization
50 problem was solved using a global deterministic solver. More recently, Gilassi
51 et al. (2019) proposed an MINLP model to find the global optimal layout
52 and operating decisions for CO_2/CH_4 separations. The authors also used the
53 model to determine the optimal values for packing fraction and dimensions
54 of a hollow fiber module. Demirel et al. (2021) utilized the “building block”
55 approach to synthesize membrane separation processes and demonstrated
56 their approach through case studies of gas and liquid binary separations. In
57 addition to deterministic optimization approaches, metaheuristic techniques
58 have also been used (Gabrielli et al., 2017; Shafiee et al., 2017; Yuan et al.,
59 2014) to solve the superstructure optimization problem for binary mixtures.
60 While approximating multicomponent as binary mixtures is sometimes ac-
61 ceptable, this simplification can lead to serious errors with respect to the
62 required membrane area (Rautenbach and Dahm, 1985).

63 Optimization approaches for multicomponent mixture separation with
64 membrane systems have been reported in literature. Qi and Henson (2000)
65 proposed an MINLP model of a fully-connected superstructure where the
66 permeators were described by an approximate model based on the funda-
67 mental transport equations. The optimization model was solved using a lo-
68 cal optimizer to design spiral-wound membrane systems separating CO_2 and
69 H_2S from crude natural gas mixtures. Mores et al. (2018) proposed an NLP
70 model to synthesize two-stage membrane systems for H_2 separation from

71 a four-component mixture. In their approach, the connections among the
72 two stages are fixed, heat exchangers after compressors/vacuum pumps are
73 employed, the pressure at each membrane side is constant, and mass trans-
74 port in the membrane module is obtained through backward finite difference
75 method (BDFM). Hasan et al. (2012) presented an NLP model for CO₂ cap-
76 ture using a restricted superstructure where each permeator was modeled
77 using a discretization-based model proposed by Uppaluri et al. (2004) and
78 solved the resulting model using a local solver. Other studies (Marriott and
79 Sørensen, 2003; Ramírez-Santos et al., 2018; Uppaluri et al., 2006) employ
80 metaheuristic approaches to solve the synthesis problem.

81 The currently available optimization approaches in this area identify lo-
82 cal optima, whereas those which achieve global optimality are too restrictive
83 (e.g., consider binary feed mixture or fixed configurations). Global optimiza-
84 tion approaches are needed since locally optimized systems may result in sig-
85 nificantly inferior solutions (Velasco et al., 2021). Furthermore, these studies
86 consider only one inlet and two outlets. More efficient membrane-based sep-
87 arations can be synthesized if a generalized representation is adopted where
88 inputs and outputs are not too restricted (Ryu et al., 2020; Kong and Mar-
89 avelias, 2020).

90 In this paper, we present a deterministic global optimization approach
91 to synthesize membrane systems for multicomponent gas mixture separa-
92 tions. To represent numerous possible configurations, we employ a super-
93 structure with rich interconnections between stages. We propose an opti-
94 mization model to find a configuration and operating conditions which re-
95 sult in minimum cost. The resulting optimization model is a nonconvex

96 MINLP which is generally challenging to solve; hence, to retain computa-
97 tional tractability, we use a physics-based surrogate unit model to describe
98 the membrane permeators. In addition to the conventional problem state-
99 ment where only one inlet and two outlets are considered, we introduce feed
100 variability by considering variable number of inlets and outlets depending on
101 the potential interconnections between the membrane system and the other
102 systems. This general problem can be used to address problems in which
103 there are alternative inlet streams due to the presence of trade-offs between
104 the difficulty/cost of the reactor network versus the separation network.

105 **2. Mathematical Formulation**

106 In the following subsections, we state the synthesis problem along with
107 the assumptions used in this work and present an optimization model which
108 consists of constraints for (1) a multicomponent permeator unit model, (2)
109 a superstructure representation of membrane systems, and (3) compressor
110 power calculation.

111 *2.1. Problem Statement*

112 The conventional problem, where a feed mixture enters a membrane sys-
113 tem outputting permeate and retentate product streams, can be stated as
114 follows. We are given:

- 115 1. a feed stream (i.e., pressure and molar flowrate of each component)
- 116 2. the membrane perm-selectivity
- 117 3. a range of admissible operating pressure ratio
- 118 4. some specifications on product streams (e.g., recovery and purity of
119 some components)

120 5. maximum number of stages

121 The aim is to find the optimal membrane system configuration, along
122 with operating conditions, which results in minimum total annual cost. The
123 model we propose is based on the following assumptions: (1) permeation
124 through the membrane material can be sufficiently described by solution-
125 diffusion mechanism; (2) ideal gas behavior; (3) the permeance of each gas
126 component is independent of the pressure and the composition of the mix-
127 ture; (4) concentration polarization is negligible; and (5) only transmembrane
128 pressure drop is observed. Most of the commercial membranes used in gas
129 separations are polymeric, so assumption (1) is valid. Assumption (2) implies
130 isothermal condition in the permeator, whereas if real gas characteristics are
131 exhibited, Joule-Thompson effect would be observed in the permeation caus-
132 ing a change in temperature from the feed- to the permeate-side (Pan, 1986).
133 Due to assumption (3), we treat permeances as constants in our formula-
134 tion. Assumption (4) allows us to approximate the concentration near the
135 membrane surface as the bulk concentration. Assumption (5) implies that
136 the pressure drops at both permeator sides and between permeation stages
137 are negligible. In subsection 2.2.3, we show that the last assumption can
138 be relaxed to handle cases where the pressure drop at the permeate-side is
139 described by nonlinear equations.

140 In generalized problem statement, the number and flowrates of influent
141 and effluent streams are allowed to vary. This generalization allows us to
142 address problems in which there are trade-offs between the membrane-based
143 separation system and other systems. We demonstrate this generalized prob-
144 lem statement in one of the examples.

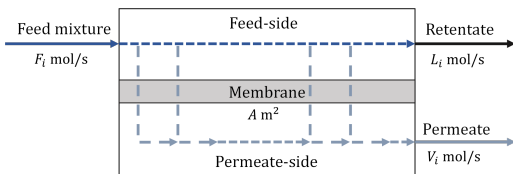


Figure 1: A membrane permeator module. Here, A is the required membrane area, while F_i, L_i , and V_i are the molar flowrates of component i in the feed, retentate, and permeate stream, respectively.

145 2.2. Permeator Model

146 In a membrane permeator, there are two compartments separated by a
 147 barrier: feed-side and permeate-side. A gas mixture enters the feed-side
 148 compartment at a high pressure, and some of the components penetrate
 149 the membrane and are collected from the permeate-side compartment as
 150 *permeate*. The remaining gas mixture is collected as *retentate*. A simplified
 151 permeator module can be seen in Figure 1. Throughout this paper, we employ
 152 $i \in \mathbf{I}$ to denote components in the feed stream and $n \in \mathbf{N}$ to denote stages
 153 in a multistage membrane system and use tilde and dot modifiers on flow
 154 variables to denote summation over $n \in \mathbf{N}$ and $i \in \mathbf{I}$, respectively.

155 If the membrane used in the permeator follows a solution-diffusion mech-
 156 anism, the transmembrane molar flux of component i , N_i , can be described
 157 by the solution-diffusion model (Wijmans and Baker, 1995):

$$N_i = \pi_i P^F (X_i - G Y_i) \quad i \in \mathbf{I} \quad (1)$$

158 where π_i is the permeance of component i in the membrane, P^F is the pres-
 159 sure on the feed-side, G is the ratio of pressure on the permeate-side to
 160 the feed-side, and X_i/Y_i is the molar fraction of component i on the feed-
 161 side/permeate-side. The above equation holds when: (1) thermodynamic

162 equilibrium exists at the fluid-membrane interfaces, (2) the solubility and
163 the diffusivity of the gas molecules in the membrane are independent of
164 pressure and temperature, (3) the external mass-transfer resistances are neg-
165 ligible. For a given stage cut (i.e., a fraction of feed which is collected as
166 permeate), the flow pattern in a permeator can significantly affect the re-
167 quired membrane area to perform a separation task. There are four idealized
168 flow patterns in membrane modules: perfect mixing, counter-current flow,
169 co-current flow, and crossflow (Oishi et al., 1961; Weller and Steiner, 1950).
170 Due to their widespread use in industry, we focus on two patterns: crossflow
171 and counter-current flow.

172 If a binary gas mixture is considered, with some simplifying assumptions,
173 analytical solutions for the unit model can be obtained. However, this is not
174 possible for multicomponent gas mixture permeations. Multicomponent per-
175 meator unit models are usually described by a Differential-Algebraic Equa-
176 tions (DAE) system, and these equations cannot be readily integrated into
177 an optimization model. Accordingly, in the following sections, we present
178 physics-based surrogate models for multicomponent permeator for crossflow
179 and counter-current flow patterns. The reformulation steps in the develop-
180 ment of both models are provided since they have a significant impact on
181 computational performance.

182 *2.2.1. Crossflow Permeator*

183 In an idealized crossflow module, the gas mixture on the feed-side passes
184 in plug flow with no longitudinal mixing. Some gas molecules from this
185 mixture penetrate the membrane and reach the permeate side without im-
186 mediately mixing with the permeate bulk flow. A simple schematic for this

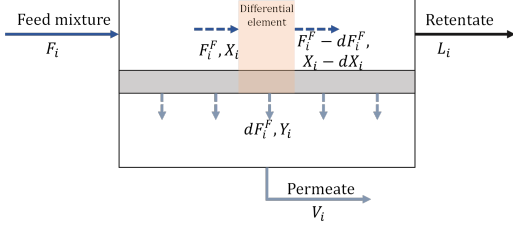


Figure 2: A membrane permeator module with crossflow pattern. Here, F_i^F is the molar flowrate of component i on the feed-side entering the differential element. The molar flowrate of component i in the feed/retentate/permeate stream is represented by $F_i/L_i/V_i$.

187 module can be seen in Figure 2.

188 The governing equations for a crossflow module based on the material
 189 balance and the transmembrane flux are as follows (Shindo et al., 1985):

$$\frac{dF_i^F}{d\dot{F}^F} = Y_i \quad i \in \mathbf{I} \quad (2)$$

$$-\frac{dF_i^F}{d\dot{A}} = \pi_i P^F (X_i - GY_i) \quad i \in \mathbf{I} \quad (3)$$

190 with the following boundary conditions:

$$F_i^F \Big|_{\dot{F}^F = \hat{F}} = F_i \quad i \in \mathbf{I} \quad (4)$$

$$\hat{F} = \sum_{i \in \mathbf{I}} F_i \quad (5)$$

191 Differential equation (2) describes the material balance around the differ-
 192 ential element, while differential equation (3) is essentially equation (1) with
 193 flux N_i replaced by molar flowrate F_i^F and area \hat{A} terms. By dividing differ-
 194 ential equation (3) by its summation over $i \in \mathbf{I}$, we obtain the term $dF_i^F/d\dot{F}^F$
 195 which can be substituted into equation (2). The resulting algebraic equation
 196 is (Shindo et al., 1985):

$$Y_i = \frac{\pi_i (X_i - GY_i)}{\sum_{i \in \mathbf{I}} \pi_i P^F (X_i - GY_i)} = \frac{\pi_i X_i}{\sum_{i \in \mathbf{I}} \pi_i P^F (X_i - GY_i) + \pi_i G} \quad i \in \mathbf{I} \quad (6)$$

If we assume that the pressure drop in both compartments is negligible and there exists an effective collective driving force which corresponds to the final stage cut, the above differential-algebraic equations (DAE) system (i.e., equations (2),(4),(5), and (6)) can be transformed into differential equations. First, we substitute the term Y_i in equation (2) with the expression in equation (6). Next, we express the equation in terms of component i molar flowrate, the feed molar flowrate \dot{F} , and the stage cut \tilde{C} . Finally, we use auxiliary variable \tilde{B} to represent the collective driving force and rearrange the differential equation. These steps can be seen below.

$$\begin{aligned}
\frac{dF_i^F}{d\dot{F}^F} &= \frac{\pi_i}{\sum_{i \in \mathbf{I}} \pi_i P^F(X_i - GY_i) + \pi_i G} \cdot X_i & i \in \mathbf{I} \\
\frac{dF_i^F}{d(\dot{F}(1 - \tilde{C}))} &= \frac{\pi_i}{\sum_{i \in \mathbf{I}} \pi_i P^F(X_i - GY_i) + \pi_i G} \cdot \frac{F_i^F}{\dot{F}(1 - \tilde{C})} & i \in \mathbf{I} \\
dF_i^F &= \frac{\pi_i}{\tilde{B} + \pi_i G} \cdot \frac{F_i^F}{1 - \tilde{C}} d(1 - \tilde{C}) & i \in \mathbf{I} \\
\frac{1}{F_i^F} dF_i^F &= \frac{\pi_i}{\tilde{B} + \pi_i G} \cdot \frac{1}{1 - \tilde{C}} d(1 - \tilde{C}) & i \in \mathbf{I} \quad (*)
\end{aligned}$$

197 Integrating differential equation (*) from $\tilde{C} = 0$ and $F_i^F = F_i$, to $\tilde{C} = C$ and
198 $F_i^F = L_i$ results in the following equation:

$$\ln \frac{L_i}{F_i} = \int_1^{1-C} \frac{\pi_i}{\tilde{B} + \pi_i G} \frac{1}{1 - \tilde{C}} d(1 - \tilde{C})$$

199 where C is the final stage cut of the permeator. By integrating the right-hand
200 side of the equation by parts, we have:

$$\begin{aligned}
\ln \frac{L_i}{F_i} &= \left[\frac{\pi_i \ln(1 - \tilde{C})}{\tilde{B} + \pi_i G} \right]_{\tilde{B}=B^0, \tilde{C}=0}^{\tilde{B}=B^L, \tilde{C}=C} + \int_{\tilde{B}=B^0, \tilde{C}=0}^{\tilde{B}=B^L, \tilde{C}=C} \frac{\pi_i \ln(1 - \tilde{C})}{(\tilde{B} + \pi_i G)^2} d\tilde{B} \\
&= \frac{\pi_i \ln(1 - C)}{B^L + \pi_i G} + I_i
\end{aligned} \tag{7}$$

201 where I_i is an integral term specific to component i and B^0/B^L is the col-
 202 lective driving force at the start/end of the permeator. Using an effective
 203 driving force B , we can approximate the above equation using the following
 204 (Chen et al., 2020):

$$\ln \frac{L_i}{F_i} = \frac{\pi_i}{B + \pi_i G} \ln(1 - C) \quad i \in \mathbf{I} \quad (8)$$

205 The final stage cut C satisfies the following relationship:

$$\sum_{i \in \mathbf{I}} L_{i,n} = (1 - C) \sum_{i \in \mathbf{I}} F_{i,n} \quad (9)$$

206 The validity of the effective driving force assumption can be evaluated
 207 by comparing the driving force from equations (7) and (8). The following
 208 relationship describes our assumption:

$$B \approx \dot{B}_i \quad i \in \mathbf{I}$$

209 where:

$$\dot{B}_i = \frac{\pi_i (B^L + \pi_i G) \ln(1 - C)}{(B^L + \pi_i G) I_i + \pi_i \ln(1 - C)} - \pi_i G \quad i \in \mathbf{I} \quad (10)$$

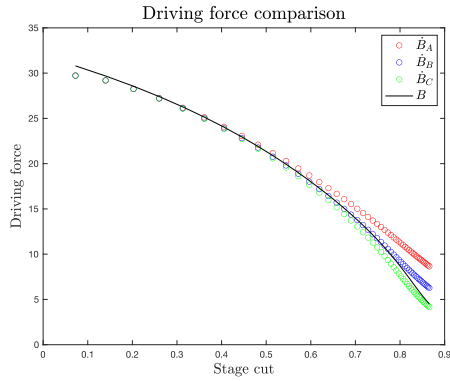
210 Through simulation (input data is provided in Table 1), we compare the
 211 values of \dot{B}_i for each component with B . To calculate B we solve a system of
 212 nonlinear equations consisting of equations (8) and (9), while to compute \dot{B}_i
 213 using equation (10) we use the solution of the DAE system (equations (2),
 214 (4), (5), and (6)) where the value of I_i is obtained using numerical integration.
 215 The comparison can be seen in Figure 3. The value of B in each example is
 216 in good agreement with the values of \dot{B}_i , suggesting that the effective driving
 217 force B is a good approximation.

Table 1: Input data for permeators

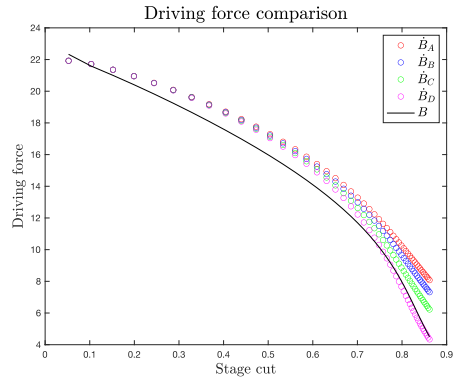
Input	Permeator 1	Permeator 2
\mathbf{I}	$\{A, B, C\}$	$\{A, B, C, D\}$
$\pi_A/\pi_B/\pi_C$	100/20/1	100/50/20/1
$F_A/F_B/F_C$	40/40/20	10/30/40/20

218 To calculate the required membrane area, we take the summation over
 219 $i \in \mathbf{I}$ of equation (3), substitute in B , and integrate the resulting differential
 220 equation from $\hat{A} = 0$ and $F_i^F = F_i$ to $\hat{A} = A$ and $F_i^F = L_i$. The steps are
 221 shown below:

$$\begin{aligned}
 -\sum_i \frac{dF_i^F}{d\hat{A}} &= -\frac{d\dot{F}^F}{d\hat{A}} = P^F \sum_i \pi_i (X_i - GY_i) \\
 -d\dot{F}^F &= P^F B d\hat{A} \\
 \dot{F} - \dot{L} &= P^F B A
 \end{aligned} \tag{11}$$



(a) Permeator 1.



(b) Permeator 2.

Figure 3: Comparison of driving forces.

222 In a multistage membrane system, the final set of constraints describing
 223 a crossflow membrane permeator at stage n is:

$$\ln(\hat{C}_n + \epsilon) = \ln(D_{i,n} + \epsilon)E_{i,n} \quad i \in \mathbf{I} \quad (\text{CF.1})$$

$$E_{i,n} = \frac{1}{\pi_i}B_n + G_n \quad i \in \mathbf{I} \quad (\text{CF.2})$$

$$L_{i,n} = D_{i,n}F_{i,n} \quad i \in \mathbf{I} \quad (\text{CF.3})$$

$$\dot{L}_n = \hat{C}_n\dot{F}_n \quad (\text{CF.4})$$

$$F_{i,n} = L_{i,n} + V_{i,n} \quad i \in \mathbf{I} \quad (\text{CF.5})$$

$$\dot{V}_n = A_n P^F B_n \quad (\text{CF.6})$$

$$\dot{F}_n = \sum_{i \in \mathbf{I}} F_{i,n} \quad (\text{CF.7})$$

$$\dot{L}_n = \sum_{i \in \mathbf{I}} L_{i,n} \quad (\text{CF.8})$$

$$\dot{V}_n = \sum_{i \in \mathbf{I}} V_{i,n} \quad (\text{CF.9})$$

224 Equation (CF.1) is obtained by rearranging equation (8) while three auxiliary
 225 variables are introduced: $E_{i,n}$ to denote the inverse of the term preceding the
 226 logarithmic term in equation (8); $D_{i,n}$ to denote the fraction of component i in
 227 the feed stream which leaves as retentate; and \tilde{C}_n to denote the complement
 228 of the final stage cut (i.e., $\tilde{C}_n = 1 - C_n$). The definitions of these three vari-
 229 ables are included as equations (CF.2), (CF.3), and (CF.4). Here, ϵ is a small
 230 number added to avoid $\ln 0$ in equation (CF.1). In this model, $F_{i,n}/L_{i,n}/V_{i,n}$
 231 represents the molar flowrate of the module feed/retentate/permeate stream,
 232 and A_n is the required membrane area. Equations (CF.5) and (CF.6) describe
 233 the material balance around the permeator and the calculation of the required
 234 membrane area, respectively. The remaining equations are the calculations
 235 of total flowrates of feed, retentate, and permeate streams. A permeator

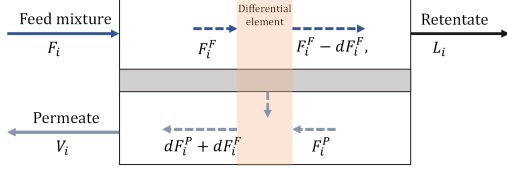


Figure 4: A membrane permeator module with counter-current flow pattern. Here, F_i^P is the molar flowrate of component i on the permeate-side entering the differential element.

236 model for multicomponent liquid separation is included in Appendix A1.

237 2.2.2. Counter-current Permeator

238 The feed-side and the permeate-side streams in a counter-current flow
 239 module flows in the opposite direction, and both streams are moving in plug
 240 flow without longitudinal mixing. The schematic of this module can be seen
 241 in Figure 4.

242 The governing equations for a counter-current module are based on the
 243 material balance and the transmembrane flux (Pettersen and Lien, 1994):

$$F_i = L_i + V_i \quad i \in \mathbf{I} \quad (12)$$

$$-\frac{dF_i^F}{d\hat{A}} = \pi_i P^F (X_i - \hat{G}Y_i) \quad i \in \mathbf{I} \quad (13)$$

244 with the following boundary conditions:

$$F_i^F \Big|_{\hat{F}^F=\hat{L}} = L_i \quad i \in \mathbf{I} \quad (14)$$

$$F_i^P \Big|_{\hat{F}^F=\hat{L}} = 0 \quad i \in \mathbf{I} \quad (15)$$

$$\frac{F_i^P}{\hat{F}^P} \Big|_{\hat{F}^F=\hat{L}} = \frac{\pi_i (X_i^R - \bar{G}\bar{Y}_i)}{\sum_{i \in \mathbf{I}} \pi_i (X_i^R - \bar{G}\bar{Y}_i)} \quad i \in \mathbf{I} \quad (16)$$

245 Here, \hat{G} and \bar{G} are variables denoting pressure ratio at each differential el-
 246 ement and at the closed-end, respectively, while X_i^R/\bar{Y}_i is the molar con-
 247 centration of component i on the feed-/permeate-side at the closed-end. By

248 assuming that the driving force (i.e., partial pressure difference) is a linear
 249 function of the change in the component molar flow on the feed-side, we ob-
 250 tain the following set of algebraic equations (more on the derivation can be
 251 found in the literature (Davis, 2002)):

$$T_i = \frac{\ddot{T}_i - \dot{T}_i}{\ln(\ddot{T}_i/\dot{T}_i)} = \frac{(X_i^R - \bar{G}\bar{Y}_i) - (X_i^F - GY_i^P)}{\ln(X_i^R - \bar{G}\bar{Y}_i) - \ln(X_i^F - GY_i^P)} \quad i \in \mathbf{I} \quad (17)$$

$$V_i = \pi_i T_i P^F A \quad i \in \mathbf{I} \quad (18)$$

252 where X_i^F/Y_i^P is the molar concentration of component i in the feed/per-
 253 meate stream. The pressure ratio at the closed end \bar{G} is calculated using
 254 pressure drop equations. Equation (16) defines the log-mean driving force T_i
 255 where \dot{T}_i and \ddot{T}_i are the driving forces of component i at the open and closed
 256 end. This equation can be approximated using Paterson's (1984) or Chen's
 257 (1987) equation to avoid numerical difficulty. In equation (17), variable \ddot{T}_i is
 258 calculated using \bar{Y}_i which is described in equation (16):

$$\bar{Y}_i = \frac{F_i^P}{\dot{F}^P} \Big|_{\dot{F}^P = \dot{L}} = \frac{\pi_i(X_i^R - \bar{G}\bar{Y}_i)}{\sum_{i \in \mathbf{I}} \pi_i(X_i^R - \bar{G}\bar{Y}_i)} \Leftrightarrow \bar{Y}_i = \frac{\pi_i X_i^R}{\sum_{i \in \mathbf{I}} \pi_i(X_i^R - \bar{G}\bar{Y}_i) + \pi_i \bar{G}} \quad i \in \mathbf{I} \quad (19)$$

259 Variable \bar{Y}_i only appears in the driving force calculation, so we can exclude
 260 this variable from our model by substituting in this variable from equation
 261 (19):

$$\ddot{T}_i = X_i^R - \bar{G}\bar{Y}_i \quad i \in \mathbf{I} \quad (20)$$

$$\begin{aligned} &= X_i^R \left(1 - \frac{\pi_i \bar{G}}{\sum_i \pi_i \dot{T}_i + \pi_i \bar{G}} \right) \quad i \in \mathbf{I} \\ &= X_i^R \left(\frac{\sum_i \pi_i \dot{T}_i}{\sum_i \pi_i \dot{T}_i + \pi_i \bar{G}} \right) \quad i \in \mathbf{I} \end{aligned} \quad (21)$$

$$\ddot{T}_i \bar{B}_i = X_i^R \quad i \in \mathbf{I} \quad (22)$$

$$\bar{B}_i = 1 + \frac{\pi_i \bar{G}}{\sum_i \pi_i \dot{T}_i} \quad i \in \mathbf{I}$$

262 Here, we use auxiliary variable \bar{B}_i to represent the inverse of the term follow-
 263 ing X_i^R in equation (21). Furthermore, we use additional auxiliary variables
 264 (\bar{E} and \bar{D}) to reduce the number of equations with bilinear terms:

$$\bar{B}_i = 1 + \pi_i \bar{E} \quad i \in \mathbf{I} \quad (23)$$

$$\bar{D} \bar{E} = \bar{G} \quad (24)$$

$$\bar{D} = \sum_i \pi_i \ddot{T}_i \quad (25)$$

265 We can now use equations (22)-(25) instead of (19) and (20). If the pres-
 266 sure drop on the permeate-side is negligible (i.e., $\bar{G} = G$), the final set of
 267 constraints describing a counter-current membrane permeator at stage n is:

$$\bar{B}_{i,n} = 1 + \pi_i \bar{E}_n \quad i \in \mathbf{I} \quad (\text{CC.1})$$

$$G_n = \bar{D}_n \bar{E}_n \quad (\text{CC.2})$$

$$\bar{D}_n = \sum_{i \in \mathbf{I}} \pi_i \ddot{T}_{i,n} \quad (\text{CC.3})$$

$$X_{i,n}^R = \ddot{T}_{i,n} \bar{B}_{i,n} \quad i \in \mathbf{I} \setminus \{\mathbf{I}\} \quad (\text{CC.4})$$

$$\sum_{i \in \mathbf{I}} \ddot{T}_{i,n} = 1 - G_n \quad (\text{CC.5})$$

$$\dot{T}_{i,n} = X_{i,n}^F - G Y_{i,n}^P \quad i \in \mathbf{I} \setminus \{\mathbf{I}\} \quad (\text{CC.6})$$

$$\sum_{i \in \mathbf{I}} \dot{T}_{i,n} = 1 - G_n \quad (\text{CC.7})$$

$$2T_{i,n}^{0.3275} = \dot{T}_{i,n}^{0.3275} + \ddot{T}_{i,n}^{0.3275} \quad i \in \mathbf{I} \quad (\text{CC.8})$$

$$V_{i,n} = \pi_i T_{i,n} P^F A_n \quad i \in \mathbf{I} \quad (\text{CC.9})$$

$$F_{i,n} = L_{i,n} + V_{i,n} \quad i \in \mathbf{I} \quad (\text{CC.10})$$

$$F_{i,n} = X_{i,n}^F \dot{F}_n \quad i \in \mathbf{I} \setminus \{\mathbf{I}\} \quad (\text{CC.11})$$

$$L_{i,n} = X_{i,n}^R \dot{L}_n \quad i \in \mathbf{I} \setminus \{\mathbf{I}\} \quad (\text{CC.12})$$

$$V_{i,n} = Y_{i,n}^P \dot{V}_n \quad i \in \mathbf{I} \setminus \{\mathbf{I}\} \quad (\text{CC.13})$$

$$\dot{F}_n = \sum_{i \in \mathbf{I}} F_{i,n} \quad (\text{CC.14})$$

$$\dot{L}_n = \sum_{i \in \mathbf{I}} L_{i,n} \quad (\text{CC.15})$$

$$\dot{V}_n = \sum_{i \in \mathbf{I}} V_{i,n} \quad (\text{CC.16})$$

$$\sum_{i \in \mathbf{I}} X_{i,n}^F = 1 \quad (\text{CC.17})$$

$$\sum_{i \in \mathbf{I}} X_{i,n}^R = 1 \quad (\text{CC.18})$$

$$\sum_{i \in \mathbf{I}} Y_{i,n}^P = 1 \quad (\text{CC.19})$$

268 Equations (CC.1)-(CC.5) are essentially equations (22)-(25), where (CC.5)
 269 is obtained by taking summation over all components of both equation sides.
 270 Similarly, equations (CC.6) and (CC.7) define the driving force at the open-
 271 end. Equations (CC.8) and (CC.9) are equations (17) and (18), respectively,
 272 but, here, Chen's approximation is used for the logarithmic-mean. The re-
 273 maining equations describe the material balance around the permeator.

274 2.2.3. Pressure Drop on the Permeate Side

275 If a more realistic unit model is required, a pressure drop equation can be
 276 included in the model. This equation is specific to the type of the permeator
 277 used; for example, the pressure drop in spiral-wound module is calculated
 278 using parameters which are different from those used in the calculation of
 279 pressure drop in hollow-fiber modules. We may use known correlations or
 280 known equations such as Darcy's Law or Hagen-Poiseuille equation to de-
 281 scribe the pressure drop on the permeate side. Accordingly, we need to make
 282 the following modifications to equation (CF.2) for crossflow permeators or
 283 equations (CC.2) and (CC.5) for countercurrent flow permeators:

$$E_{i,n} = \frac{1}{\pi_i} B_n + \bar{G}_n \quad i \in \mathbf{I} \quad (\text{CF.2a})$$

$$\bar{G}_n = \bar{D}_n \bar{E}_n \tag{CC.2a}$$

$$\sum_{i \in \mathbf{I}} \ddot{T}_{i,n} = 1 - \bar{G}_n \tag{CC.5a}$$

284 For crossflow permeators, \bar{G}_n is the ratio of the pressure at the mem-
 285 brane surface on the permeate side to the pressure of the feed-side bulk
 286 stream; while for counter-current flow permeators, it is the pressure ratio of
 287 the permeate-side to the feed-side bulk streams at the closed end.

288 In addition, an equation to describe the pressure drop is also required.
 289 For example, if we have a hollow-fiber permeator with permeate in the tube-
 290 side, the following equation can be added to describe the pressure drop at
 291 stage n :

$$\bar{G}_n^2 = G_n^2 + \hat{\xi} A_n \dot{V}_n$$

292 where $\hat{\xi}$ is a parameter which depends on the internal of the permeator.

293 *2.3. Superstructure Representation*

294 We use a superstructure with rich interconnections which allows (1) fresh
 295 feed to be sent to any stage, (2) a retentate to be sent to any of the next stages
 296 as a bypass stream, (3) a permeate to be sent to any of the previous stages
 297 as a recycle stream, (4) a retentate product to be collected from any stage,
 298 and (5) a permeate product to be collected from any stage. Here, the recycle
 299 streams must be compressed to match the feed pressure. A superstructure
 300 for a four-stage membrane system is shown in Figure 5.

301 In the mathematical formulation of the superstructure, the existence of
 302 stages and connections are represented by binary variables. Binary variable
 303 Z_n is introduced to indicate if stage n is active. To avoid symmetric solutions,

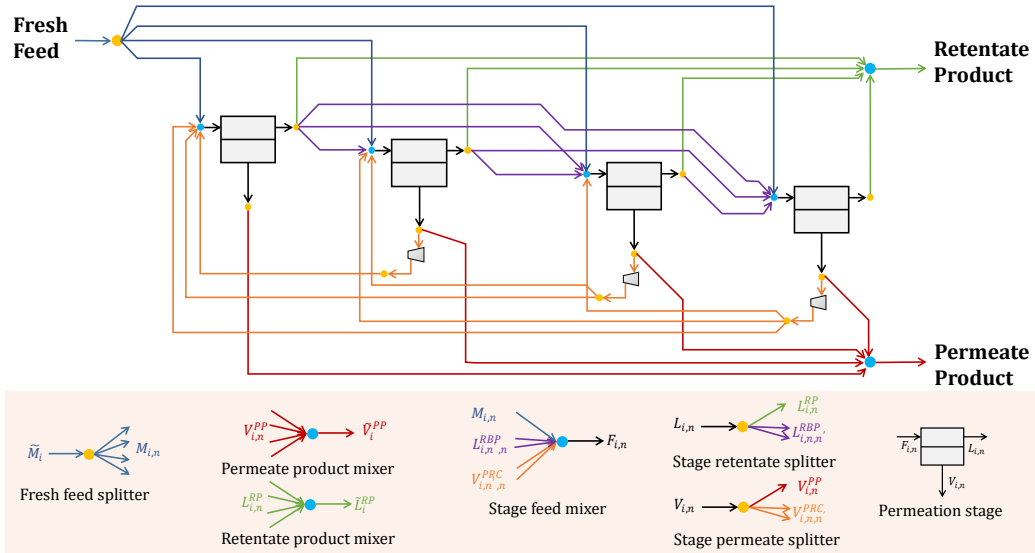


Figure 5: Superstructure representation for membrane systems. Blue and yellow disks represent mixers and splitters, respectively.

304 we use a constraint to deactivate the succeeding stages if the current stage
 305 is inactive.

$$Z_n \geq Z_{n+1} \quad n \in \mathbf{N} \setminus \{|\mathbf{N}|\} \quad (26)$$

306 We also introduce binary variable \hat{Z}_n to indicate if fresh feed enters stage n .
 307 Since this stream enters only one stage and that stage must be active, we
 308 include the following constraints:

$$\sum_{n \in \mathbf{N}} \hat{Z}_n = 1 \quad (27)$$

$$\sum_{n'=n}^{|\mathbf{N}|} \hat{Z}_{n'} \leq Z_n \quad n \in \mathbf{N} \quad (28)$$

309 The molar flowrate of component i in the feed mixture, \tilde{M}_i , is disag-
 310 gregated into continuous variable $M_{i,n}$ for every stage n using the following

311 constraints:

$$\sum_{n \in \mathbf{N}} M_{i,n} = \tilde{M}_i \quad i \in \mathbf{I} \quad (29)$$

$$\sum_{i \in \mathbf{I}} M_{i,n} \leq \phi^{UB} \hat{Z}_n \quad n \in \mathbf{N} \quad (30)$$

312 where ϕ^{UB} is an upper bound for molar flowrates. The above constraints will
 313 result in only one positive disaggregated fresh feed stream.

314 To represent the existence of a bypass and a recycle streams from stage
 315 n to stage n' , we introduce binary variables $W_{n,n'}^{RBP}$ and $W_{n,n'}^{PRC}$, respectively,
 316 whose values become 1 if those connections exist. Note that we have $W_{n,n'}^{RBP}$
 317 only for $n < n'$ and $W_{n,n'}^{PRC}$ only for $n > n'$. Finally, binary variables W_n^{RP}
 318 and W_n^{PP} are introduced to indicate if retentate and permeate product, re-
 319 spectively, are collected from stage n . In this superstructure representation,
 320 the retentate is either collected as final retentate product or sent to one of
 321 the next stages, while the permeate is either collected as final permeate prod-
 322 uct or recycled to one of the previous stages. We introduce two subsets to
 323 denote all stages after and before stage n : $\mathbf{N}_n^> := \{n' \in \mathbf{N} | n' > n\}$ and
 324 $\mathbf{N}_n^< := \{n' \in \mathbf{N} | n' < n\}$.

$$\sum_{n' \in \mathbf{N}_n^>} W_{n,n'}^{RBP} + W_n^{RP} = Z_n \quad n \in \mathbf{N} \quad (31)$$

$$\sum_{n' \in \mathbf{N}_n^<} W_{n,n'}^{PRC} + W_n^{PP} = Z_n \quad n \in \mathbf{N} \quad (32)$$

325 This superstructure representation uses $|\mathbf{N}| + 2$ mixers (1 for each feed
 326 entering stage n and 1 for each final product) and $3|\mathbf{N}| + 1$ splitters (1 for
 327 each retentate leaving stage n , 2 for each permeate leaving stage n , and 1
 328 for the fresh feed stream). The material balance around the mixer for feed

329 entering stage n can be written as:

$$F_{i,n} = M_{i,n} + \sum_{n' \in \mathbf{N}_n^>} V_{i,n',n}^{PRC} + \sum_{n' \in \mathbf{N}_n^<} L_{i,n',n}^{RBP} \quad i \in \mathbf{I}, n \in \mathbf{N} \quad (33)$$

330 where $V_{i,n',n}^{PRC}/L_{i,n',n}^{RBP}$ is the molar flowrate of component i in permeate/ret-
 331 entate stream from stage n' which is recycled/bypassed to stage n . The
 332 material balances for final products are:

$$\tilde{L}_i^{RP} = \sum_n L_{i,n}^{RP} \quad i \in \mathbf{I} \quad (34)$$

$$\tilde{V}_i^{PP} = \sum_n V_{i,n}^{PP} \quad i \in \mathbf{I} \quad (35)$$

333 where $\tilde{L}_i^{RP}/\tilde{V}_i^{PP}$ is the molar flowrate of component i in the retentate/per-
 334 meate final product, while $L_{i,n}^{RP}/V_{i,n}^{PP}$ is the molar flowrate of component i
 335 in the retentate/permeate final product collected from stage n . The mate-
 336 rial balance around the splitter for the fresh feed mixture is represented by
 337 constraint (29) and those around splitters for retentate and permeate leaving
 338 stage n are described by the following constraints:

$$L_{i,n} = L_{i,n}^{RP} + \sum_{n' \in \mathbf{N}_n^>} L_{i,n,n'}^{RBP} \quad i \in \mathbf{I}, n \in \mathbf{N} \quad (36)$$

$$V_{i,n} = V_{i,n}^{PP} + \sum_{n' \in \mathbf{N}_n^<} V_{i,n,n'}^{PRC} \quad i \in \mathbf{I}, n \in \mathbf{N} \quad (37)$$

339 Note that despite the use of two splitters for each permeate stream in Fig-
 340 ure 5, the material balance can be represented by one splitter as shown in
 341 constraint (37). Finally, big-M constraints are introduced so that a molar
 342 flowrate may only be nonzero when the corresponding connection exists.

$$\sum_{i \in \mathbf{I}} L_{i,n}^{RP} \leq \phi^{UB} W_n^{RP} \quad n \in \mathbf{N} \quad (38)$$

$$\sum_{i \in \mathbf{I}} V_{i,n}^{PP} \leq \phi^{UB} W_n^{PP} \quad n \in \mathbf{N} \quad (39)$$

$$\sum_{i \in \mathbf{I}} V_{i,n,n'}^{PRC} \leq \phi^{UB} W_{n,n'}^{PRC} \quad n' \in \mathbf{N}_n^{\leq}, n \in \mathbf{N} \quad (40)$$

$$\sum_{i \in \mathbf{I}} L_{i,n,n'}^{RBP} \leq \phi^{UB} W_{n,n'}^{RBP} \quad n' \in \mathbf{N}_n^{>}, n \in \mathbf{N} \quad (41)$$

343 We also require all permeate streams collected as permeate product to have
 344 a specified pressure.

$$345 \quad \frac{P^P}{P^F} - \gamma^{UB}(1 - W_n^{PP}) \leq G_n \leq \frac{P^P}{P^F} + \gamma^{UB}(1 - W_n^{PP}) \quad n \in \mathbf{N} \quad (42)$$

346 where P^P is the pressure of the permeate product and γ^{UB} is the upper
 347 bound of the pressure ratio. Constraint (42) ensures that the pressure of
 348 permeate stream matches the pressure of the permeate product if $W_n^{PP}=1$.

349 For the generalized problem, where the number and flows of inlet and
 350 outlet streams are allowed to vary, we relax the superstructure shown in
 351 Figure 5 by increasing the number of fresh feed splitters and final product
 352 mixers depending on the potential interconnections with the other systems.
 353 Furthermore, note that any black-box unit model can be employed in con-
 354 junction with the proposed framework as long as the model can describe
 355 the input-output relations required in the proposed superstructure model
 356 adequately.

357 2.4. Power Calculation

358 The existence of recycle streams in the superstructure requires recom-
 359 pressing the permeate streams to match the feed pressure P^F . If isentropic
 360 compression is assumed, the compressor power W_n^{CP} can be calculated using
 361 the following constraints:

$$W_n^{CP} + S_n = \delta \dot{V}_n (H_n - 1) \quad n \in \mathbf{N} \quad (43)$$

$$H_n = \beta \ln G_n \quad n \in \mathbf{N} \quad (44)$$

$$W_n^{CP} \leq \delta \phi^{UB} (\gamma^{UB\beta} - 1) (Z_n - W_n^{PP}) \quad n \in \mathbf{N} \quad (45)$$

$$S_n \leq \delta \phi^{UB} (\gamma^{UB\beta} - 1) W_n^{PP} \quad n \in \mathbf{N} \quad (46)$$

362 where δ is a parameter calculated from the universal gas constant, temper-
 363 ature of the permeate stream, gas isentropic coefficient, and efficiency and
 364 β is an exponent calculated from gas isentropic coefficient. In the above
 365 constraints, we introduce an auxiliary variable H_n (defined in equation (44))
 366 and a positive slack variable S_n . Due to equations (43), (45), and (46), W_n^{CP}
 367 will only be positive if there is a permeate recycle stream leaving stage n .

368 **3. Solution Methods**

369 Although the constraints in section 2 are sufficient to describe the mem-
 370 brane system, the resulting optimization model is challenging to solve. More-
 371 over, the constraints describing the superstructure may also include some
 372 symmetric configurations. Therefore, solution methods such as tightening
 373 constraints and variable bounds are required in order to expedite the solu-
 374 tion process (Kong et al., 2016). In the following subsections, we present
 375 variable bounds and tightening constraints both for general and specific per-
 376 meator types that we found helpful.

377 *3.1. Variable Bounds*

378 *3.1.1. Crossflow Permeator Unit Model Specific Bounds*

379 The complement of the final stage cut \hat{C}_n denotes the fraction of entering
 380 molar flowrate which leaves as retentate. In an inactive stage, both entering

381 and exiting flowrates are 0; however, since \hat{C}_n appears only in bilinear terms
 382 in the optimization model, we may include the following bounds:

$$\hat{\zeta}^{LB} \leq \hat{C}_n \leq \hat{\zeta}^{UB} \quad n \in \mathbf{N} \quad (47)$$

383 where $\hat{\zeta}^{LB}$ can be a small number close to 0 and $\hat{\zeta}^{UB}$ can be a number close
 384 to 1. Requiring the stage cut to be between these bounds does not force
 385 the optimization model to activate a stage since this variable appears in a
 386 bilinear term multiplied with molar flowrates.

387 In the derivation of equation (*), we defined auxiliary variable B_n as:

$$B_n = \sum_{i \in \mathbf{I}} \pi_i (X_i - GY_i) \quad n \in \mathbf{N}$$

388 From the above, it is obvious that B_n will always be less than the permeance
 389 of the fastest component. On the other hand, we can obtain a lower bound
 390 from an extreme case where the stage cut is close to 1; thus, the remaining
 391 gas is mostly the slowest species. The bounds for B_n are as follows:

$$\min_{i \in \mathbf{I}} \pi_i \leq B_n \leq \max_{i \in \mathbf{I}} \pi_i \quad n \in \mathbf{N} \quad (48)$$

392 Using the bounds for B_n in equation (48) and the definition of $E_{i,n}$ in equation
 393 (CF.2), we can derive the following bounds for auxiliary variable $E_{i,n}$:

$$\frac{\min_{i \in \mathbf{I}} \pi_i}{\pi_i} + \gamma^{LB} \leq E_{i,n} \leq \frac{\max_{i \in \mathbf{I}} \pi_i}{\pi_i} + \gamma^{UB} \quad i \in \mathbf{I}, n \in \mathbf{N} \quad (49)$$

394 where γ^{LB} is the lower bound for pressure ratio. Finally, using the bounds
 395 on complement of the final stage cut \hat{C}_n and auxiliary variable $E_{i,n}$, we can
 396 derive the following bounds:

$$\hat{\zeta}^{LB} \frac{\pi_i}{\min_{i \in \mathbf{I}} \pi_i + \pi_i \gamma^{LB}} \leq D_{i,n} \leq \hat{\zeta}^{UB} \frac{\pi_i}{\max_{i \in \mathbf{I}} \pi_i + \pi_i \gamma^{UB}} \quad i \in \mathbf{I}, n \in \mathbf{N} \quad (50)$$

397 Note that, using the same reasoning as in the derivation of equation (47),
 398 these variables have physical meaning only when the stage associated with
 399 them is active; thus, providing reasonable lower and upper bounds on them
 400 will not affect the optimal solution.

401 3.1.2. Counter-current Flow Permeator Unit Model Specific Bounds

402 Using the equation describing counter-current flow permeator in subsec-
 403 tion 2.2.2, we can derive bounds on the variables involved in bilinear terms.
 404 First, we introduce bounds on the molar concentrations.

$$0 \leq X_{i,n}^F \leq 1 \quad i \in \mathbf{I}, n \in \mathbf{N} \quad (51)$$

$$0 \leq X_{i,n}^R \leq 1 \quad i \in \mathbf{I}, n \in \mathbf{N} \quad (52)$$

$$0 \leq Y_{i,n}^P \leq 1 \quad i \in \mathbf{I}, n \in \mathbf{N} \quad (53)$$

405 In the counter-current flow permeator, the driving force of each com-
 406 ponent is the difference of concentration on the feed-side and a product of
 407 concentration on the permeate-side and the pressure ratio; thus, we can set
 408 the following bounds:

$$0 \leq T_{i,n} \leq 1 - \gamma^{LB} \quad i \in \mathbf{I}, n \in \mathbf{N} \quad (54)$$

$$0 \leq \dot{T}_{i,n} \leq 1 - \gamma^{LB} \quad i \in \mathbf{I}, n \in \mathbf{N} \quad (55)$$

$$0 \leq \ddot{T}_{i,n} \leq 1 - \gamma^{LB} \quad i \in \mathbf{I}, n \in \mathbf{N} \quad (56)$$

409 From equation (CC.3), we can have the following bounds for \bar{D}_n :

$$\min_{i \in \mathbf{I}} \pi_i \leq \bar{D}_n \leq \max_{i \in \mathbf{I}} \pi_i \quad n \in \mathbf{N} \quad (57)$$

410 *3.2. Tightening Constraints*

411 *3.2.1. Superstructure*

412 Tightening constraints can be formulated for the molar flowrates at the
 413 permeate and retentate splitters. Using the corresponding binary variables,
 414 we can include the following constraints:

$$L_{i,n,n'}^{RBP} \geq L_{i,n} - \phi^{UB}(1 - W_{n,n'}^{RBP}) \quad i \in \mathbf{I}, n' \in \mathbf{N}_n^>, n \in \mathbf{N} \quad (58)$$

$$L_{i,n}^{RP} \geq L_{i,n} - \phi^{UB}(1 - W_n^{RP}) \quad i \in \mathbf{I}, n \in \mathbf{N} \quad (59)$$

$$V_{i,n,n'}^{PRC} \geq V_{i,n} - \phi^{UB}(1 - W_{n,n'}^{PRC}) \quad i \in \mathbf{I}, n' \in \mathbf{N}_n^<, n \in \mathbf{N} \quad (60)$$

$$V_{i,n}^{PP} \geq V_{i,n} - \phi^{UB}(1 - W_n^{PP}) \quad i \in \mathbf{I}, n \in \mathbf{N} \quad (61)$$

415 We can also write constraints for the stage inlets. If a permeate recycle or
 416 retentate bypass stream enters that stage, then that stage is active.

$$Z_n \leq \hat{Z}_n + \sum_{n'>n} W_{n',n}^{PRC} + \sum_{n'<n} W_{n',n}^{RBP} \quad n \in \mathbf{N} \quad (62)$$

$$Z_n \geq W_{n',n}^{PRC} \quad n' \in \mathbf{N}_n^>, n \in \mathbf{N} \quad (63)$$

$$Z_n \geq W_{n',n}^{RBP} \quad n' \in \mathbf{N}_n^<, n \in \mathbf{N} \quad (64)$$

417 Moreover, we can remove configurations that are symmetric or will not be
 418 optimal. If there is no stream flowing between a pair of stages n and \hat{n} and
 419 between any of those stages and any stage in between, then stage n and \hat{n} are
 420 interchangeable. To break the symmetry, we differentiate these two stages in
 421 crossflow/countercurrent permeators system using their stage cut/required
 422 area by introducing the following constraints:

$$C_n \geq \hat{C}_{\hat{n}} - \left(W_{n,\hat{n}}^{RBP} + W_{n,\hat{n}}^{PRC} + \sum_{n < n' < \hat{n}} W_{n,n'}^{RBP} + W_{n',\hat{n}}^{RBP} + W_{n',n}^{PRC} + W_{\hat{n},n'}^{PRC} \right) \quad \hat{n} \in \mathbf{N}_n^<, n \in \mathbf{N} \quad (65)$$

$$A_n \geq A_{\hat{n}} - \alpha \left(W_{n,\hat{n}}^{RBP} + W_{n,\hat{n}}^{PRC} + \sum_{n < n' < \hat{n}} W_{n,n'}^{RBP} + W_{n',\hat{n}}^{RBP} + W_{n',n}^{PRC} + W_{\hat{n},n'}^{PRC} \right) \quad \hat{n} \in \mathbf{N}_n^<, n \in \mathbf{N} \quad (66)$$

423 where α is the upper bound for required membrane area.

424 Symmetric solutions can also be obtained if fresh feed is the only stream
 425 entering a stage: we obtain the same solution by placing this stage anywhere
 426 after the stage connected with its permeate recycle stream and before the
 427 stage which receives its retentate bypass stream. To remove this symmetry,
 428 we introduce the following constraints:

$$W_n^{PP} - \left(\sum_{n' \in \mathbf{N}_n^<} W_{n',n}^{RBP} + \sum_{n' \in \mathbf{N}_n^>} W_{n',n}^{PRC} \right) \leq \hat{Z}_n$$

$$\leq W_n^{PP} + \left(\sum_{n' \in \mathbf{N}_n^<} W_{n',n}^{RBP} + \sum_{n' \in \mathbf{N}_n^>} W_{n',n}^{PRC} \right) \quad n = 1 \quad (67)$$

$$W_{n,n-1}^{PRC} - \left(\sum_{n' \in \mathbf{N}_n^<} W_{n',n}^{RBP} + \sum_{n' \in \mathbf{N}_n^>} W_{n',n}^{PRC} \right) \leq \hat{Z}_n$$

$$\leq W_{n,n-1}^{PRC} + \left(\sum_{n' \in \mathbf{N}_n^<} W_{n',n}^{RBP} + \sum_{n' \in \mathbf{N}_n^>} W_{n',n}^{PRC} \right) \quad 1 < n \leq |\mathbf{N}| \quad (68)$$

429 In the proposed membrane system, a series of recycle/bypass streams
 430 concentrate fast/slow components. Since we are separating some fast/slow
 431 component from a mixture subject to purity specifications, the permeate/re-
 432 tentate final product will be collected from the first/final few stages since the
 433 permeates/retentates leaving these stages will have a higher concentration of
 434 that component compared to other stages. Moreover, it is highly unlikely
 435 that a product stream is not collected from a stage if the product stream

436 is also collected from the previous and following stages. Accordingly, the
 437 following constraints can be added into the optimization model:

$$W_{n+1}^{PP} \leq W_n^{PP} \quad n \in \mathbf{N} \setminus \{|\mathbf{N}|\} \quad (69)$$

$$W_{n-1}^{RP} \leq W_n^{RP} + (1 - Z_n) \quad n \in \mathbf{N} \setminus \{1\} \quad (70)$$

438 In constraint (70), a term with Z_n is included to ensure that this constraint
 439 is valid only if that stage is active.

440 Finally, for crossflow membrane systems, we want to exclude solutions
 441 containing two permeators connected by a bypass stream sending both permeate
 442 streams to a single location (as a recycle or permeate product) if no
 443 other streams enter the later permeator since this configuration can be represented
 444 by a single permeator.

$$W_{n,\hat{n}}^{PRC} - W_{\hat{n},\hat{n}}^{PRC} \leq 2 - W_{n,\hat{n}}^{RBP} + \hat{Z}_n + \left(\sum_{\substack{n' \neq n \\ n' \in \mathbf{N}_{\hat{n}}^<}} W_{n',\hat{n}}^{RBP} + \sum_{n' \in \mathbf{N}_{\hat{n}}^>} W_{n',\hat{n}}^{PRC} + \hat{Z}_{\hat{n}} \right) \quad \hat{n} \in \mathbf{N}_n^<, \hat{n} \in \mathbf{N}_n^>, n \in \mathbf{N} \quad (71)$$

$$W_n^{PP} - W_{\hat{n}}^{PP} \leq 2 - W_{n,\hat{n}}^{RBP} + \hat{Z}_n + \left(\sum_{\substack{n' \neq n \\ n' \in \mathbf{N}_{\hat{n}}^<}} W_{n',\hat{n}}^{RBP} + \sum_{n' \in \mathbf{N}_{\hat{n}}^>} W_{n',\hat{n}}^{PRC} + \hat{Z}_{\hat{n}} \right) \quad \hat{n} \in \mathbf{N}_n^>, n \in \mathbf{N} \quad (72)$$

445 3.2.2. Crossflow Permeator Unit Model

446 We can derive tightening constraints based on our physical understanding
 447 of the system. As stated in Section 2, B_n is an auxiliary variable related to
 448 the collective driving force at stage n . When a bypass connection between
 449 stage n and n' is established, we know that the average feed-side molar

450 fraction of the fastest species at stage n is greater than that at stage n' .
 451 Since the value of B_n is proportional to the product of molar fraction and
 452 permeance, smaller average feed-side molar fraction of the fastest species
 453 leads to a smaller value of B_n . Following the same logic, we also derive a
 454 constraint for recycle streams.

$$B_n \leq B_{n'} + \left(\max_{i \in \mathbf{I}} \pi_i - \min_{i \in \mathbf{I}} \pi_i \right) W_{n,n'}^{PRC} \quad n' \in \mathbf{N}_n^<, n \in \mathbf{N} \quad (73)$$

$$B_n \geq B_{n'} - \left(\max_{i \in \mathbf{I}} \pi_i - \min_{i \in \mathbf{I}} \pi_i \right) W_{n,n'}^{RBP} \quad n' \in \mathbf{N}_n^>, n \in \mathbf{N} \quad (74)$$

455 If the permeances of components are in descending order, we can have the
 456 following constraints:

$$D_{1,n} \leq C_n \leq D_{|\mathbf{I}|,n} \quad n \in \mathbf{N} \quad (75)$$

$$D_{i,n} \leq D_{i+1,n} \quad i \in \mathbf{I} \setminus \{|\mathbf{I}|\}, n \in \mathbf{N} \quad (76)$$

457 Inequality (75) can be derived from equations (CF.3) and (CF.5), while in-
 458 equality (76) can be derived from (CF.1) and (CF.2).

459 3.2.3. Counter-current Flow Permeator Unit Model

460 In each permeator, the molar fraction of a component in the feed stream
 461 is between those in the retentate and permeate streams; thus, we can write
 462 the following constraints for the most and least permeable components.

$$X_{1,n}^R \leq X_{1,n}^F \leq Y_{1,n}^P \quad n \in \mathbf{N} \quad (77)$$

$$Y_{|\mathbf{I}|,n}^P \leq X_{|\mathbf{I}|,n}^F \leq X_{|\mathbf{I}|,n}^R \quad n \in \mathbf{N} \quad (78)$$

463 Using equation (CC.1), the following equation can be written.

$$\bar{B}_{i,n} \geq \bar{B}_{i+1,n} \quad i \in \mathbf{I} \setminus \{|\mathbf{I}|\}, n \in \mathbf{N} \quad (79)$$

464 Since we have a bilinear term in equation (CC.6), we introduce a convex
 465 underestimator and overestimator using the pressure ratio upper and lower
 466 bounds:

$$X_{i,n}^F - \gamma^{UB} Y_{i,n}^P \leq \dot{T}_{i,n} \leq X_{i,n}^F - \gamma^{LB} Y_{i,n}^P \quad i \in \mathbf{I}, n \in \mathbf{N} \quad (80)$$

467 Additional constraints can be derived based on our physical understanding
 468 of the system, where: (1) the retentate molar fraction of the most/least
 469 permeable component decreases/increases from a stage to another stage if
 470 these stages are connected by a retentate bypass stream and (2) the permeate
 471 molar fraction of the most/least permeable component increases/decreases
 472 from a stage to another stage if these stages are connected by a permeate
 473 recycle stream.

$$X_{1,n}^R \geq X_{1,n'}^R - (1 - W_{n,n'}^{RBP}) \quad n' \in \mathbf{N}_n^>, n \in \mathbf{N} \quad (81)$$

$$X_{|\mathbf{I}|,n}^R \leq X_{|\mathbf{I}|,n'}^R - (1 - W_{n,n'}^{RBP}) \quad n' \in \mathbf{N}_n^>, n \in \mathbf{N} \quad (82)$$

$$Y_{1,n}^P \leq Y_{1,n'}^P - (1 - W_{n,n'}^{PRC}) \quad n' \in \mathbf{N}_n^<, n \in \mathbf{N} \quad (83)$$

$$Y_{|\mathbf{I}|,n}^P \geq Y_{|\mathbf{I}|,n'}^P - (1 - W_{n,n'}^{PRC}) \quad n' \in \mathbf{N}_n^<, n \in \mathbf{N} \quad (84)$$

474 Furthermore, since the logarithmic mean is used in the driving force equation,
 475 the relationship of arithmetic and logarithmic means can be added:

$$T_{i,n} \leq \frac{\dot{T}_{i,n} + \ddot{T}_{i,n}}{2} \quad i \in \mathbf{I}, n \in \mathbf{N} \quad (85)$$

476 4. Illustrative Examples

477 We present two examples to demonstrate the applicability of the proposed
 478 models. The first example demonstrates the modularity of our formulation

479 where crossflow or counter-current flow permeators can be used in the super-
480 structure and pressure drop can be included if needed. The second example,
481 which is based on small integrated reactor-separation system, shows how the
482 model can be used to address a generalized problem statement where the
483 feed is no longer fixed, and the outlet streams are not restricted to two. All
484 models are formulated in GAMS 35.1.0 on a Windows machine with 3 GHz
485 CPU and 8 GB RAM. The relative tolerance for convergence is set to 0.05.

486 *4.1. Natural Gas Sweetening*

487 We use the case study presented by Qi and Henson (2000). In this exam-
488 ple, 10 mol/s of raw natural gas mixture containing 19% CO₂, 1% H₂S, 73%
489 CH₄, and 7% heavier hydrocarbons C₂₊ is fed into the membrane system to
490 reduce the CO₂ content to 2% (which is the specification of pipeline grade
491 gas). The feed-side pressure of the membrane system is the same as the
492 pressure of the fresh feed that is 3.5 MPa, while the permeate-side pressure
493 may vary as long as the final permeate product is collected at 0.105 MPa.
494 Finally, isothermal compression is assumed for this process. Other param-
495 eters used for this case study (e.g., cost coefficients and operating conditions)
496 are obtained from that reference (Qi and Henson, 2000). In this case study,
497 the objective is to minimize the annual process cost (in \$/1000m³) which
498 depends on the membrane area, compressor power, and methane losses.

499 The flowsheet for a three-stage system reported by Qi and Henson (2000)
500 can be seen in Figure 6 with an objective function value of 10.971 \$/1000m³.
501 In that solution, a spiral-wound permeator approximate model is used to de-
502 scribe the multicomponent gas permeation. This model was shown to be very
503 accurate when compared to the DAE-based model (Qi and Henson, 1997).

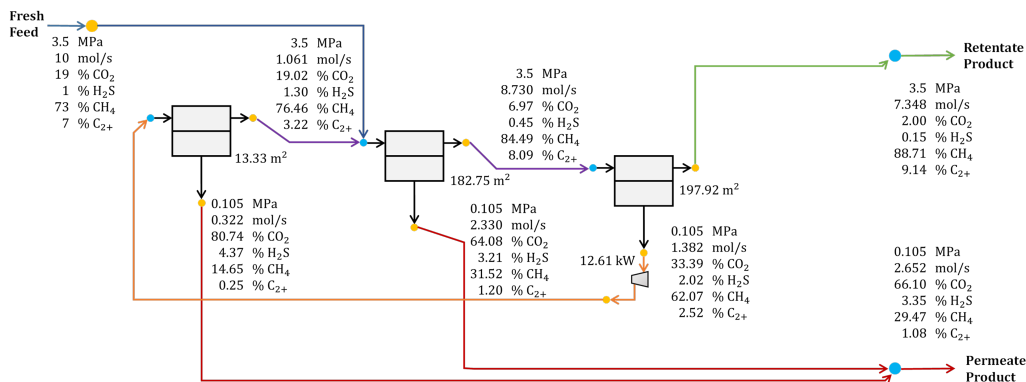


Figure 6: Three-stage permembrane system reported by Qi and Henson (2000).

504 Using the same parameters and final product specifications, we solve the syn-
 505 thesis problem using two types of permeators: crossflow and counter-current
 506 flow. The best solutions for crossflow and counter-current flow can be seen in
 507 Figure 7 and Figure 8, respectively. The optimization model using the cross-
 508 flow membrane unit model has 293 equations and 176 variables (18 binaries).
 509 It is solved to 5% optimality in 1,185 s using SCIP 7.0 (Gamrath et al., 2020),
 510 an off-the-shelf global optimization solver based on spatial branch-and-bound
 511 algorithm using linear relaxation, resulting in a configuration which is the
 512 same as the one obtained by Qi and Henson (2000) but with a lower objective
 513 function value of 8.501 \$/1000m³. On the other hand, the model using the
 514 counter-current flow membrane system has 445 equations and 236 variables
 515 (18 binaries) and is solved to 5% optimality in 2,986 s yielding solution with
 516 an objective function value of 8.342 \$/1000m³. Interestingly, we observe
 517 that the best solution obtained using crossflow permeators and that using
 518 counter-current flow permeators are similar in their molar flowrates, area,
 519 and energy requirement, which is also observed by Yang et al. (2017).

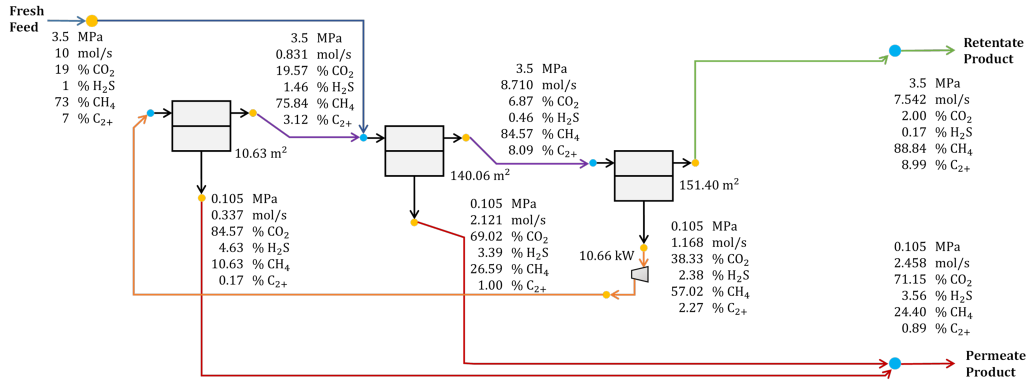


Figure 7: Best solution for three-stage crossflow-type permeator system.

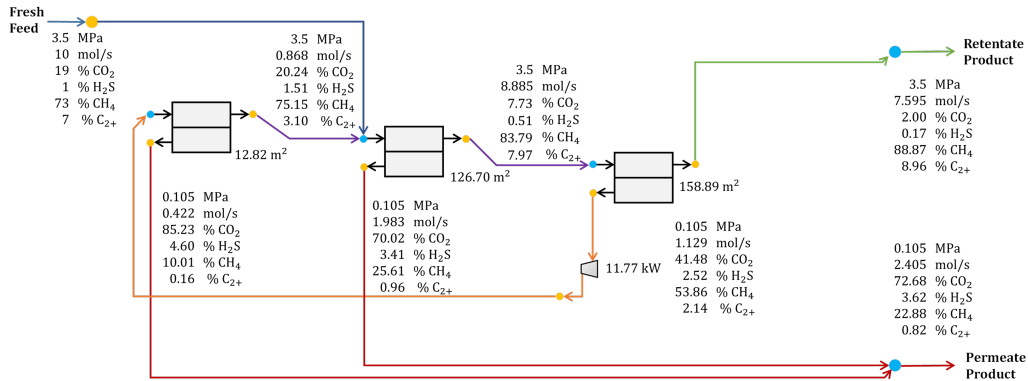


Figure 8: Best solution for three-stage countercurrent flow-type permeator system.

520 The difference in objective value obtained in this work and that from the
 521 reference (Qi and Henson, 2000) is partly because of the underestimation of
 522 the required area due to assuming negligible pressure drop. When pressure
 523 drop is accounted in the crossflow membrane system (by adapting the pres-
 524 sure drop correlation provided by Qi and Henson (2000)), the optimization
 525 model has 296 equations and 179 variables (18 binaries) and is solved to
 526 5% optimality gap in 1,874 s using SCIP with an objective function value of
 527 10.914 \$/1000m³ and a configuration as shown in Figure 9. The result of this

528 model compares favorably with that from reference (Qi and Henson, 2000)
 529 with slight differences due to the modeling of the permeators. Furthermore,
 530 we now treat the feed-side pressure in the system as variable which introduces
 531 a trade-off between the required membrane area and the compressor power.
 532 Here, the fresh feed is available at atmospheric pressure (0.105 MPa), and
 533 the upper bound for the feed-side pressure is set at 5 MPa. The model for
 534 this problem has 294 equations and 181 variables (18 binaries) and is solved
 535 in 2,767 s using SCIP with an objective function value of 16.109 \$/1000m³.
 536 The feed-side pressure in the best solution (see Figure 10) is at its bound,
 537 while the configuration is identical to the configurations with fixed feed-side
 538 pressure. The same observation was made by Qi and Henson (2000).

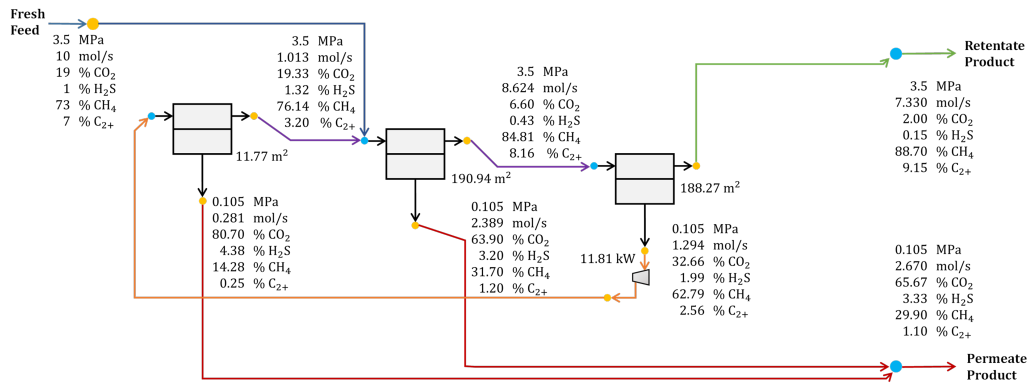


Figure 9: Best solution for three-stage crossflow-type permeator system with pressure drop.

539 Finally, Qi and Henson (2000) assume isothermal compression. Here, we
 540 solve the problem again assuming isentropic compressors ($\delta = 11.57 \frac{\text{kW}}{\text{mol/s}}$ and
 541 $\beta = -0.26$). The optimization model for a maximum number of three stages
 542 and pressure drop has 299 equations and 182 variables (18 binaries) and is

543 solved to 5% optimality within 3,201 s yielding a solution (see Figure 11)
 544 with an objective function value of 11.488 \$/1000m³. In this solution, only
 545 two stages are employed despite setting the maximum number of stages to
 546 three.

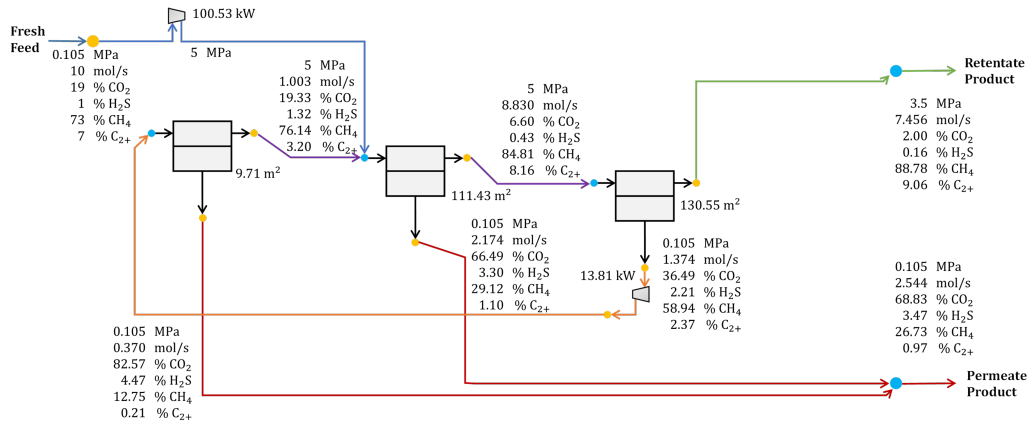


Figure 10: Best solution for three-stage crossflow-type permeator system with pressure drop and variable feed-side pressure.

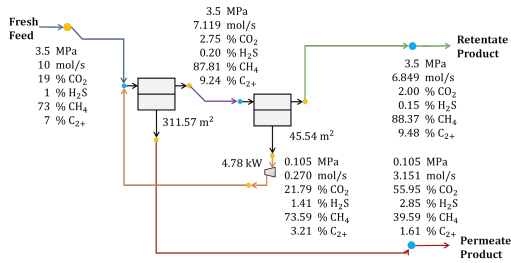


Figure 11: Best solution for crossflow-type permeator system with pressure drop and isentropic compressors.

547 4.2. Integrated Reactor-Separation System

548 We use a small integrated reactor-separation system which produces component *C*
 549 from reactant *A*. Two reaction routes are available: (1) direct reac-

550 tion, $A \rightarrow 0.5C$; (2) reaction which involves an intermediate, $A \rightarrow B \rightarrow 0.5C$.
 551 The first option has a fixed conversion of 60%, while the second option has
 552 fixed conversions of 85% and 95% for the first and second reaction, respec-
 553 tively. The effluent of the reactor is then sent to a membrane system to
 554 recover 100 mol/s permeate product stream with 98.5% C . The retentate
 555 stream can be recycled and mixed with pure A as the reactor feed or treated
 556 as waste. That stream can be recycled only if the molar fraction of compo-
 557 nent A in the reactor influent stream is at least 75%. The option to dispose
 558 the retentate product is offered in case the cost of concentrating unreacted A
 559 due to more compression and membrane area required is higher than the cost
 560 reduction from recycling the reactant. A simple schematic of the integrated
 561 system can be seen in Figure 12.

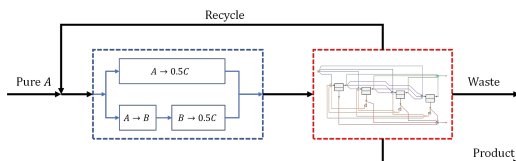


Figure 12: Integrated reactor-separation system.

562 We assume that the pressure drop in both permeator compartments is
 563 negligible and isentropic compressors are used. The objective function is the
 564 minimization of the annualized cost (in $\frac{\$/\text{yr}}{\text{mol permeate product/s}}$) which includes
 565 costs associated with the required compression and membrane area, molar
 566 flowrates of components entering the reactor, and the purchased pure A :

$$\text{Annualized cost} = \frac{\omega^{CP} \sum_{n \in \mathbf{N}} W_n^{CP} + \omega^{MP} \sum_{n \in \mathbf{N}} A_n + \sum_{r \in \mathbf{R}} \omega_{i,r}^{RX} \bar{F}_{i,r} + \omega^F \bar{F}_A}{\sum_{i \in \mathbf{I}} V_{i,n}^{PP}}$$

567 where $r \in \mathbf{R}$ represents reaction route options, \bar{F}_A is molar flowrate of
 568 pure component A which enters the integrated system, and $\bar{F}_{i,r}$ is molar

569 flowrate of component i in the reactor influent stream which undergoes re-
 570 action(s) in route r . The economic parameters and operating conditions
 571 pertaining to this example can be found in Table 2. The molar flowrates
 572 of stream entering the membrane system varies depending on the chosen
 573 reaction route and the recycle stream if selected. This example exhibits a
 574 trade-off between the cost of reactor and separation system. The first reac-
 575 tion route has higher cost and lower conversion, but the separation is easier
 576 due to the absence of the intermediate, whereas the second reaction route
 577 has lower cost and higher conversion but it produces an intermediate which
 leads to a more difficult and costlier separation.

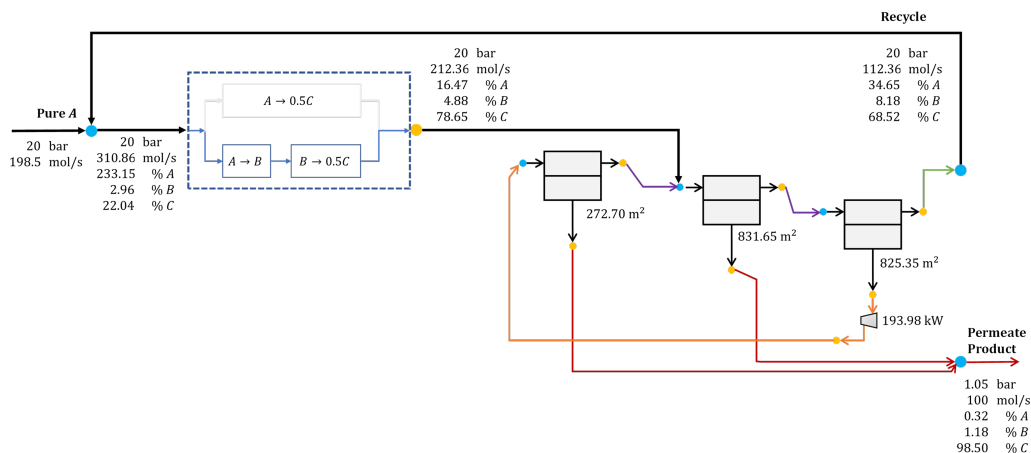


Figure 13: Solution for integrated reactor-separation system toy case.

578

579 The solution does not only give the best configuration of the membrane
 580 system, but also the selection of the reaction route and decision to recycle.
 581 Using the model introduced in section 2 for crossflow permeators, we for-
 582 mulate a model with 297 equations and 187 variables (23 binaries), which is
 583 solved in 664 seconds using SCIP 7.0 to 5% optimality gap. The annualized

584 cost of the best solution is \$9,209/(mol/s product). The second reactor route
585 is chosen and the retentate final product from the membrane system is sent
586 back and mixed with pure A to be fed into the reactor. The solution for this
587 integrated system can be seen in Figure 13.

Table 2: Operating conditions and economic parameters.

Parameter	Value	Description
ω^{CP}	700	Annualized cost parameter for compression (\$/kW/yr)
ω^{MP}	100	Annualized cost parameter for permeators (\$/m ² /yr)
$\omega_{A,r1}^{RX}/\omega_{A,r2}^{RX}/\omega_{B,r2}^{RX}$ $/\omega_{C,r1}^{RX}/\omega_{C,r2}^{RX}$	500/300/200 /2500/1000	Annualized cost parameter for reactors (\$/yr/(mol/s))
ω^F	2000	Purchase price of pure A (\$/yr/(mol/s))
P^F/P^P	20/1.05	Feed-side/permeate product pressure (bar)
$\pi_A/\pi_B/\pi_C$	0.001/0.01/0.06	Permeance (mol/MPa/m ² /s)
δ	11.57	Isentropic compressor constant (kW/(mol/s))
β	-0.26	Isentropic compressor exponent (dimensionless)

588 **5. Conclusion**

589 We presented a superstructure-based optimization approach for synthe-
590 sizing membrane systems. The approach relies on the use of physics-based
591 surrogate models for the two most used permeator flow patterns (crossflow
592 and counter-current flow) to describe permeation of multicomponent mix-
593 tures. If required, equations to describe pressure drop can be readily in-
594 cluded. A richly connected superstructure is used to allow (1) the retentate
595 of a stage to be sent forward to any of the next stages or collected as final
596 retentate product and (2) the permeate of a stage to be sent back to any of
597 previous stages or collected as final permeate product. To enhance the so-
598 lution of the resulting model, we proposed a series of tightening constraints.
599 The applicability of the model was demonstrated through a case study of
600 natural gas sweetening. Finally, we considered a generalization of the con-
601 ventional membrane system synthesis problem where the feed entering the
602 membrane system is subject to optimization and recycle streams from the
603 membrane system to the reactor system is considered.

Nomenclature

Sets

$i \in \mathbf{I}$	components
$n \in \mathbf{N}$	permeation stages
$n' \in \mathbf{N}_n^<$	permeation stages before stage n
$n' \in \mathbf{N}_n^>$	permeation stages after stage n

Parameters

α	upper bound for required membrane area
β	isentropic compressor exponent
δ	isentropic compressor constant
γ^{LB}/γ^{UB}	lower/upper bound for pressure ratio
$\hat{\xi}$	parameter which depends on the internal of the permeator
ϕ^{UB}	upper bound for molar flowrates
π_i	permeance for component i
$\hat{\zeta}^{LB}/\hat{\zeta}^{UB}$	lower/upper bound for \tilde{C}

Nonnegative Continuous Variables

$\bar{E}_{i,n}/\bar{B}_n/\bar{D}_{i,n}$	auxiliary variables specific to countercurrent flow permeators
$\dot{F}_n/\dot{L}_n/\dot{V}_n$	total feed/retentate/permeate stream molar flowrate of stage n
\tilde{C}_n	fraction of feed molar flowrate which leaves as retentate
\tilde{G}_n	transmembrane pressure ratio of the membrane surface on the permeate side to the feed-side bulk stream (for cross-flow permeator systems)/ permeate-side to the feed-side bulk streams at the closed end (for counter-current flow permeator systems)

$\tilde{L}_i^{RP}/\tilde{V}_i^{PP}$	component i molar flowrate in final retentate/permeate product
\tilde{M}_i	component i molar flowrate in fresh feed mixture
A_n	required membrane area at stage n
$E_{i,n}/B_n/D_{i,n}$	auxiliary variables specific to crossflow permeators
$F_{i,n}/L_{i,n}/V_{i,n}$	component i molar flowrate in the feed/retentate/permeate stream of stage n
G_n	pressure ratio of feed and permeate stream at stage n
H_n	auxiliary variable for compressor power calculation at stage n
$L_{i,n,n'}^{RBP}/V_{i,n,n'}^{PRC}$	component i molar flowrate in retentate bypass/permeate recycle stream from stage n to stage n'
$L_{i,n}^{RP}/V_{i,n}^{PP}$	component i molar flowrate in retentate/permeate leaving stage n which is collected as final retentate/permeate product
$M_{i,n}$	disaggregated component i molar flowrate in fresh feed mixture which enters stage n
P^F/P^P	pressure on the feed-side of permeators/pressure of the permeate product
S_n	slack variable for compressor power calculation at stage n

$T_{i,n}/\dot{T}_{i,n}/\ddot{T}_{i,n}$	log-mean/open-end/closed-end driving force of component i at stage n
W_n^{CP}	compressor power at stage n
$X_{i,n}^F/X_{i,n}^R/Y_{i,n}^P$	molar fraction of component i in the feed/retentate/permeate stream of stage n

Binary Variables

\hat{Z}_n	1 if the fresh feed mixture enters stage n
$W_{n,n'}^{RBP}/W_{n,n'}^{PRC}$	1 if there is a retentate bypass/permeate recycle stream from stage n to stage n'
W_n^{RP}/W_n^{PP}	1 if final retentate/permeate product is collected from stage n
Z_n	1 if stage n is active

Acknowledgement

This work was supported by the Great Lakes Bioenergy Research Center, U.S. Department of Energy, Office of Science, Office of Biological and Environmental Research under Award Number DE-SC0018409.

Appendix A. Crossflow Permeator Unit Model for Multicomponent Liquid Mixture Separation

Using the flux equation described by solution-diffusion model (Wijmans and Baker, 1995) for reverse osmosis:

$$N_i = \pi_i (X_i - Y_i \exp(-\nu_i G)) \quad i \in \mathbf{I}$$

where the ν_i is a lumped parameter calculated from the component molar volume, the gas constant, and the temperature. Note that, instead of the transmembrane pressure *ratio*, as in the gas separation case, variable G now denotes the transmembrane pressure *difference*. Using the same assumption, i.e., constant collective driving force along the permeator, the crossflow permeator unit model becomes:

$$\ln(\hat{C}_n + \epsilon) = \ln(D_{i,n} + \epsilon)E_{i,n} \quad i \in \mathbf{I} \quad (\text{A.1})$$

$$E_{i,n} = \frac{1}{\pi_i} B_n + \tilde{G}_n \quad i \in \mathbf{I} \quad (\text{A.2})$$

$$\ln \tilde{G}_n = -\nu_i G_n \quad (\text{A.3})$$

$$L_{i,n} = D_{i,n} F_{i,n} \quad i \in \mathbf{I} \quad (\text{A.4})$$

$$\dot{L}_n = \hat{C}_n \dot{F}_n \quad (\text{A.5})$$

$$F_{i,n} = L_{i,n} + V_{i,n} \quad i \in \mathbf{I} \quad (\text{A.6})$$

$$\dot{V}_n = A_n B_n \quad (\text{A.7})$$

$$\dot{F}_n = \sum_{i \in \mathbf{I}} F_{i,n} \quad (\text{A.8})$$

$$\dot{L}_n = \sum_{i \in \mathbf{I}} L_{i,n} \quad (\text{A.9})$$

$$\dot{V}_n = \sum_{i \in \mathbf{I}} V_{i,n} \quad (\text{A.10})$$

In the above model, \tilde{G}_n is an auxiliary variable, and it is defined in equation (A.3).

References

- Agrawal, R., Xu, J., 1996. Gas-separation membrane cascades utilizing limited numbers of compressors. *AIChE Journal* doi:10.1002/aic.690420806.
- Arias, A.M., Mussati, M.C., Mores, P.L., Scenna, N.J., Caballero, J.A., Mussati, S.F., 2016. Optimization of multi-stage membrane systems for co2 capture from flue gas. *International Journal of Greenhouse Gas Control* 53, 371–390. doi:10.1016/j.ijggc.2016.08.005.
- Castro-Dominguez, B., Leelachaikul, P., Messaoud, S.B., Takagaki, A., Sugawara, T., Kikuchi, R., Oyama, S.T., 2015. The optimal point within the robeson upper boundary. *Chemical Engineering Research and Design* 97, 109–119. doi:10.1016/j.cherd.2015.03.002.
- Chen, J.J., 1987. Comments on improvements on a replacement for the logarithmic mean. *Chemical Engineering Science* doi:10.1016/0009-2509(87)80128-8.
- Chen, Z., Gooty, R.T., Velasco, J.A.C., Tawarmalani, M., Agrawal, R., 2020. Global optimization of multicomponent membrane cascade. URL: <https://aiche.confex.com/aiche/2020/webprogram/Paper602370.html>. AIChE Annual Meeting.
- Davis, R.A., 2002. Simple gas permeation and pervaporation membrane unit operation models for process simulators. *Chemical Engineering and Technology* doi:10.1002/1521-4125(20020709)25:7<717::AID-CEAT717>3.0.CO;2-N.

- Demirel, S.E., Li, J., Hasan, M.F., 2021. Membrane separation process design and intensification. *Industrial & Engineering Chemistry Research* 60, 7197–7217. doi:10.1021/acs.iecr.0c05072.
- Du, N., Cin, M.M., Pinnau, I., Nicalek, A., Robertson, G.P., Guiver, M.D., 2011. Azide-based cross-linking of polymers of intrinsic microporosity (pims) for condensable gas separation. *Macromolecular Rapid Communications* doi:10.1002/marc.201000775.
- Gabrielli, P., Gazzani, M., Mazzotti, M., 2017. On the optimal design of membrane-based gas separation processes. *Journal of Membrane Science* 526, 118–130. doi:10.1016/j.memsci.2016.11.022.
- Gamrath, G., Anderson, D., Bestuzheva, K., Chen, W.K., Eifler, L., Gasse, M., Gemander, P., Gleixner, A., Gottwald, L., Halbig, K., et al., 2020. The scip optimization suite 7.0. Technical Report.
- Gilassi, S., Taghavi, S.M., Rodrigue, D., Kaliaguine, S., 2019. Optimizing membrane module for biogas separation. *International Journal of Greenhouse Gas Control* 83, 195–207. doi:10.1016/j.ijggc.2019.02.010.
- Grossmann, I.E., 1996. Mixed-integer optimization techniques for algorithmic process synthesis. *Advances in Chemical Engineering* doi:10.1016/S0065-2377(08)60203-3.
- Hasan, M.F., Baliban, R.C., Elia, J.A., Floudas, C.A., 2012. Modeling, simulation, and optimization of postcombustion co₂ capture for variable feed concentration and flow rate. 1. chemical absorption and membrane pro-

- cesses. *Industrial and Engineering Chemistry Research* 51, 15642–15664. doi:10.1021/ie301571d.
- Humphrey, J.L., Keller, G.E., 1997. *Separation process technology*. McGraw-Hill New York.
- Iulianelli, A., Drioli, E., 2020. Membrane engineering: Latest advancements in gas separation and pre-treatment processes, petrochemical industry and refinery, and future perspectives in emerging applications. *Fuel Processing Technology* 206, 106464. doi:10.1016/j.fuproc.2020.106464.
- Kong, L., Maravelias, C.T., 2020. Expanding the scope of distillation network synthesis using superstructure-based methods. *Computers & Chemical Engineering* 133, 106650. doi:10.1016/j.compchemeng.2019.106650.
- Kong, L., Sen, S.M., Henao, C.A., Dumesic, J.A., Maravelias, C.T., 2016. A superstructure-based framework for simultaneous process synthesis, heat integration, and utility plant design. *Computers & Chemical Engineering* 91, 68–84. doi:10.1016/j.compchemeng.2016.02.013.
- Koros, W.J., Lively, R.P., 2012. Water and beyond: Expanding the spectrum of large-scale energy efficient separation processes. *AIChE journal* 58, 2624–2633. doi:10.1002/aic.13888.
- Krovvidi, K.R., Kovvali, A.S., Vemury, S., Khan, A.A., 1992. Approximate solutions for gas permeators separating binary mixtures. *Journal of Membrane Science* doi:10.1016/0376-7388(92)87001-E.
- Marriott, J., Sørensen, E., 2003. The optimal design of membrane systems. *Chemical Engineering Science* doi:10.1016/j.ces.2003.07.011.

- McKeown, N.B., Budd, P.M., 2010. Exploitation of intrinsic microporosity in polymer-based materials. *Macromolecules* doi:10.1021/ma1006396.
- Merkel, T.C., Lin, H., Wei, X., Baker, R., 2010. Power plant post-combustion carbon dioxide capture: An opportunity for membranes. *Journal of Membrane Science* 359, 126–139. doi:10.1016/j.memsci.2009.10.041.
- Mores, P.L., Arias, A.M., Scenna, N.J., Caballero, J.A., Mussati, S.F., Mussati, M.C., 2018. Membrane-based processes: Optimization of hydrogen separation by minimization of power, membrane area, and cost. *Processes* doi:10.3390/pr6110221.
- Murad Chowdhury, M.H., Feng, X., Douglas, P., Croiset, E., 2005. A new numerical approach for a detailed multicomponent gas separation membrane model and aspenplus simulation. *Chemical Engineering and Technology* 28, 773–782. doi:10.1002/ceat.200500077.
- Ohs, B., Lohaus, J., Wessling, M., 2016. Optimization of membrane based nitrogen removal from natural gas. *Journal of Membrane Science* 498, 291–301. doi:10.1016/j.memsci.2015.10.007.
- Oishi, J., Matsumura, Y., Higashi, K., Ike, C., 1961. An analysis of gaseous diffusion separating unit. *Nippon Genshiryoku Gakkai-Shi* 3, 923–928.
- Pan, C.Y., 1983. Gas separation by permeators with high-flux asymmetric membranes. *AIChE Journal* doi:10.1002/aic.690290405.
- Pan, C.Y., 1986. Gas separation by high-flux, asymmetric hollow-fiber membrane. *AIChE Journal* doi:10.1002/aic.690321212.

- Park, H.B., Jung, C.H., Lee, Y.M., Hill, A.J., Pas, S.J., Mudie, S.T., Van Wagner, E., Freeman, B.D., Cookson, D.J., 2007. Polymers with cavities tuned for fast selective transport of small molecules and ions. *Science* doi:10.1126/science.1146744.
- Paterson, W.R., 1984. A replacement for the logarithmic mean. *Chemical Engineering Science* doi:10.1016/0009-2509(84)80090-1.
- Pettersen, T., Lien, K.M., 1994. A new robust design model for gas separating membrane modules, based on analogy with counter-current heat exchangers. *Computers and Chemical Engineering* 18, 427–439. doi:10.1016/0098-1354(94)88021-2.
- Pinnau, I., Casillas, C.G., Morisato, A., Freeman, B.D., 1996. Hydrocarbon/hydrogen mixed gas permeation in poly(1-trimethylsilyl-1-propyne) (ptmsp), poly(1-phenyl-1-propyne) (ppp), and ptmsp/ppp blends. *Journal of Polymer Science, Part B: Polymer Physics* doi:10.1002/(SICI)1099-0488(19961115)34:15<2613::AID-POLB9>3.0.CO;2-T.
- Qi, R., Henson, M.A., 1997. Modeling of spiral-wound permeators for multicomponent gas separations. *Industrial & engineering chemistry research* 36, 2320–2331.
- Qi, R., Henson, M.A., 2000. Membrane system design for multicomponent gas mixtures via mixed-integer nonlinear programming. *Computers and Chemical Engineering* 24, 2719–2737. doi:10.1016/S0098-1354(00)00625-6.
- Ramírez-Santos, Á.A., Bozorg, M., Addis, B., Piccialli, V., Castel, C., Favre, E., 2018. Optimization of multistage membrane gas separation processes.

- example of application to co2 capture from blast furnace gas. *Journal of Membrane Science* 566, 346–366. doi:10.1016/j.memsci.2018.08.024.
- Rautenbach, R., Dahm, W., 1985. The separation of multicomponent mixtures by gas permeation. *Chemical Engineering and Processing* 19, 211–219. doi:10.1016/0255-2701(84)80024-0.
- Robeson, L.M., 2008. The upper bound revisited. *Journal of Membrane Science* 320, 390–400. doi:10.1016/j.memsci.2008.04.030.
- Ryu, J., Kong, L., Pastore de Lima, A.E., Maravelias, C.T., 2020. A generalized superstructure-based framework for process synthesis. *Computers and Chemical Engineering* doi:10.1016/j.compchemeng.2019.106653.
- Shafiee, A., Nomvar, M., Liu, Z., Abbas, A., 2017. Automated process synthesis for optimal flowsheet design of a hybrid membrane cryogenic carbon capture process. *Journal of Cleaner Production* doi:10.1016/j.jclepro.2017.02.151.
- Shindo, Y., Hakuta, T., Yoshitome, H., 1985. Calculation methods for multicomponent gas separation by permeation. *Separation Science and Technology* doi:10.1080/01496398508060692.
- Spillman, R., 1995. Economics of gas separation membrane processes. *Membrane Science and Technology* 2, 589–667. doi:10.1016/S0927-5193(06)80015-X.
- Stern, S.A., Perrin, J.E., Naimon, E.J., 1984. Recycle and multimembrane permeators for gas separations. *Journal of Membrane Science* doi:10.1016/S0376-7388(00)80721-8.

- Uppaluri, R.V., Linke, P., Kokossis, A.C., 2004. Synthesis and optimization of gas permeation membrane networks. *Industrial & engineering chemistry research* 43, 4305–4322. doi:10.1021/ie030787c.
- Uppaluri, R.V., Smith, R., Linke, P., Kokossis, A.C., 2006. On the simultaneous optimization of pressure and layout for gas permeation membrane systems. *Journal of Membrane Science* 280, 832–848. doi:10.1016/j.memsci.2006.03.004.
- Velasco, J.A.C., Gooty, R.T., Tawarmalani, M., Agrawal, R., 2021. Optimal design of membrane cascades for gaseous and liquid mixtures via minlp. *Journal of Membrane Science* , 119514.
- Weller, S., Steiner, W.A., 1950. Separation of gases by fractional permeation through membranes. *Journal of Applied Physics* 21, 279–283. doi:10.1063/1.1699653.
- Wijmans, J.G., Baker, R.W., 1995. The solution-diffusion model: a review. *Journal of membrane science* 107, 1–21. doi:10.1016/0376-7388(95)00102-I.
- Yang, D., Ren, H., Li, Y., Wang, Z., 2017. Suitability of cross-flow model for practical membrane gas separation processes. *Chemical Engineering Research and Design* 117, 376–381. doi:10.1016/j.cherd.2016.10.036.
- Yuan, M., Narakornpijit, K., Haghpanah, R., Wilcox, J., 2014. Consideration of a nitrogen-selective membrane for postcombustion carbon capture through process modeling and optimization. *Journal of Membrane Science* doi:10.1016/j.memsci.2014.04.026.

Highlights

Generalized Optimization-based Synthesis of Membrane Systems for Multicomponent Gas Mixture Separation

Garry S.P. Taifan, Christos T. Maravelias

- Proposed superstructure-based optimization approach for membrane systems synthesis
- Developed new physics-based surrogate models describing permeation of multicomponent mixtures
- General problem, with variable inlet flows and recycle streams, considered
- Approach applied to address different types of mixture and problems